New Journal of Physics
The open access journal at the forefront of physics

Deutsche Physikalische Gesellschaft DPG IOP Institute of Physics

PAPER • OPEN ACCESS

Ising model for melt ponds on Arctic sea ice

To cite this article: Yi-Ping Ma *et al* 2019 *New J. Phys.* **21** 063029

New Journal of Physics
The open access journal at the forefront of physics

Deutsche Physikalische Gesellschaft DPG
IOP Institute of Physics

Published in partnership with: Deutsche Physikalische Gesellschaft and the Institute of Physics

OPEN ACCESS

RECEIVED
1 February 2019

REVISED
8 May 2019

ACCEPTED FOR PUBLICATION
4 June 2019

PUBLISHED
21 June 2019

PAPER

Ising model for melt ponds on Arctic sea ice

Yi-Ping Ma[1], **Ivan Sudakov**[2], **Courtenay Strong**[3] **and Kenneth M Golden**[4]

[1] Northumbria University, Department of Mathematics, Physics, and Electrical Engineering, Ellison Place, Newcastle upon Tyne, NE1 8ST, United Kingdom
[2] University of Dayton, Department of Physics, 300 College Park, SC 111, Dayton, OH 45469-2314, United States of America
[3] University of Utah, Department of Atmospheric Sciences, 135 S 1460 E Rm 819, Salt Lake City, UT 84112-0102, United States of America
[4] University of Utah, Department of Mathematics, 155 S 1400 E Rm 233, Salt Lake City, UT 84112-0090, United States of America

E-mail: golden@math.utah.edu

Keywords: Arctic sea ice, melt ponds, Ising model, metastable states, fractal geometry

Supplementary material for this article is available online

Abstract

Perhaps the most iconic feature of melting Arctic sea ice is the distinctive ponds that form on its surface. The geometrical patterns describing how melt water is distributed over the surface largely determine the solar reflectance and transmittance of the sea ice cover, which are key parameters in climate modeling and upper ocean ecology. In order to help develop a predictive theoretical approach to studying melting sea ice, and the resulting patterns of light and dark regions on its surface in particular, we look to the statistical mechanics of phase transitions and introduce a two-dimensional random field Ising model which accounts for only the most basic physics in the system. The ponds are identified as metastable states in the model, where the binary spin variable corresponds to the presence of melt water or ice on the sea ice surface. With the lattice spacing determined by snow topography data as the only measured parameter input into the model, energy minimization drives the system toward realistic pond configurations from an initially random state. The model captures the essential mechanism of pattern formation of Arctic melt ponds, with predictions that agree very closely with observed scaling of pond sizes and transition in pond fractal dimension.

1. Introduction

While snow and ice reflect most of the sunlight incident on Arctic sea ice, melt ponds absorb most of it. The ponds largely control the albedo, or solar reflectance of sea ice, as well as its transmittance [1–5], which in turn impact the heat and mass balances of the ice cover and the partitioning of energy in the upper ocean and lower atmosphere. The ponds play a critical role in *ice-albedo feedback*, a key mechanism in the rapid decline of the summer Arctic ice pack [6]. In fact, by accounting for ponds in climate simulations, predicted ice pack volumes are significantly lower [7], and the yearly Arctic sea ice minimum can be accurately forecast from melt pond area in spring [4]. The impact of melt pond evolution extends into the biosphere as well [8–10], where the ponds act as *windows* for light to shine into the upper ocean, affecting Arctic marine ecology. Typical pond configurations are shown in figure 1(a).

There has been significant progress on numerical models of melt pond evolution [7, 3–5], although current generation melt pond parameterizations in climate models track melt water volume, not how melt water is distributed on the ice surface. However, the geometry of melt ponds and their spatial patterns impacts various sea ice and upper ocean processes such as albedo evolution, the break-up of floes, the evolution of the floe size distribution, and the patterns of light in and under the ice, which can affect photosynthetic activity and the ecology of microbial communities.

There are two key, benchmark observations of melt pond geometry that must be accounted for by a statistical physics theory of melt ponds. The first dates back to the 1998 SHEBA expedition and the measurement of melt pond sizes from images taken from helicopters [11]. The pond size distribution function prob(A)

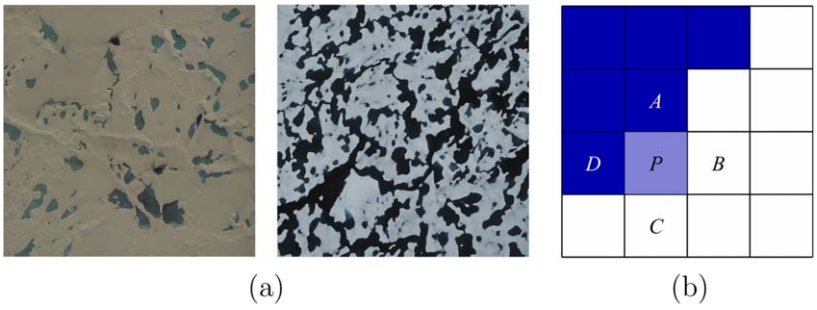

Figure 1. Melt pond configurations and the update step in Glauber dynamics. (a) Helicopter photos of melt ponds on sea ice in the western Beaufort Sea (Perovich). On the left, each side of this 15 July 1998 photo is 826 m; on the right, each side of this 14 August 2005 photo is 193 m. (b) Illustration of the tiebreaker update step in Glauber dynamics. Here each site i is assigned a pre-melt ice height h_i, and colored dark blue for water ($s_i = +1$) and white for ice ($s_i = -1$). Site P, to be updated, is adjacent to two water sites A and D, and two ice sites B and C. Since water tends to fill troughs, we require that $s_P = +1$ if $h_P < 0$, and -1 otherwise.

exhibits power law scaling $\text{prob}(A) \sim A^{\zeta}$ with the observed value of the exponent ζ for pond areas in the range $10\ \text{m}^2 < A < 1000\ \text{m}^2$ being about $-3/2$.

Area-perimeter analysis of images of melt ponds from SHEBA as well as the 2005 Healy–Oden Trans Arctic Expedition (HOTRAX) has shown that as the ponds grow and coalesce into much larger connected structures they display a transition in fractal geometry [12], evolving from simple Euclidean shapes into complex, self-similar regions whose boundaries behave like space-filling curves. The fractal dimension of the boundary curves transitions from 1 to about 2 around a critical area of about 100 m^2. In addition to constraining the geometry of melt pond evolution, the area-perimeter relationship is key to quantifying components of pond growth, such as vertical *versus* lateral melt, regulating the extent of the water-ice interface where lateral expansion of the ponds can occur.

Recent work shows that these geometrical characteristics are consistent with behavior exhibited by continuum percolation models [13–15]. In [16] a melt pond boundary is the intersection of a random surface representing the snow topography with a horizontal plane representing the water level. As the plane rises the ponds grow and coalesce. An autoregressive class of anisotropic random Fourier surfaces with correlation parameters based on snow data provides topographies that yield realistic ponds, the observed transition in fractal dimension, and a framework to analyze how the shape of the fractal transition depends on topographic characteristics.

In [17] a void model for melt ponds is introduced, where disks of varying size which represent ice and can overlap are placed randomly on the plane, with the voids between them representing the ponds. Data on pond sizes, area fractions, and correlations measured from helicopter photos of melt ponds are incorporated through parameters input into the model. The model yields the observed fractal transition and pond size distribution, and can be used to explore the generality of the behavior.

Here we address the challenge of developing a *predictive* theoretical model of melt ponds which accounts for the most basic physics of the system, and which yields realistic pond configurations obtained through minimization of the energy of the model. After all, we are interested in a solid–liquid phase transition from sea ice to sea water, albeit over large length and time scales. We turn then to the statistical mechanics of the Ising model to introduce such an approach [13, 18]. Only the most essential physics is incorporated—in the same way that the original Ising model includes only the most basic aspects of a ferromagnet in an external magnetic field.

We envision a square lattice of surface patches or *pixels* of melt water or ice, corresponding to the classical spin up or spin down states, respectively. They are collectively influenced by an external forcing field, and interact only with their nearest neighbors. The energy of the melting sea ice system is expressed similarly to how the energy of a ferromagnet is estimated in the Ising Hamiltonian. Pond-like configurations, or connected regions of 'up spins,' result from a series of energy reducing updates of an initially random state. Glauber spin flip dynamics guide the flow of configurations toward realistic melt pond states which are local energy minima, or metastable states. We remark that while we can estimate the time scale associated with a spin flip—that is, melting or freezing a surface patch under certain conditions, we are not using the present model to directly describe the time evolution of ponds over the melt season.

Our introduction of a melt pond Ising model addresses a central issue in climate science, that is, *linkage of scales*. How can knowledge of local interactions be used to predict *macroscopic* behavior relevant to large scale, coarse-grained models? This is the type of fundamental problem that is solved in statistical physics [18, 13] and homogenization for composite materials [19, 15]. Illustrating the potentially broad applicability of this

approach, an Ising model for tropical convection was developed [20] to represent atmospheric processes unresolved by coarse scale climate models.

2. Theoretical framework

First, we recall the most general form of the classical Ising free energy

$$\mathcal{H} = -\sum_i H_i s_i - \sum_{\langle i,j\rangle} J_{ij} s_i s_j, \tag{1}$$

where i ranges over a two dimensional square lattice with periodic boundary conditions, the s_i are spin variables taking the values $+1$ or -1 corresponding to spin up or spin down, and $\langle i,\ j\rangle$ denotes nearest neighbors. The parameters H_i and J_{ij} represent the external magnetic field and coupling constants, respectively. In our melt pond Ising model the state variable is a binary (or spin) variable s_i such that $s_i = +1$ corresponds to absorptive melt water on the surface of our pixelated model sea ice floe and $s_i = -1$ corresponds instead to reflective ice or snow on the surface. In addition, a temperature T can be defined which characterizes the strength of thermal fluctuations, but here we set $T = 0$ assuming for simplicity that environmental noise does not significantly influence melt pond geometry. The two dimensional nature of the Ising model we consider here is most relevant to thinner, flatter first year sea ice, rather than thicker multiyear ice where it may be more important to include three dimensional effects.

To describe nontrivial spin clustering at zero temperature, the H_i and/or J_{ij} are chosen as random variables; the resulting models are collectively known as disordered Ising models [21]. In particular, one recovers the classical random field Ising model (RFIM) if the H_i are independent random variables and the J_{ij} are constant. At zero temperature, the system is usually assumed to follow Glauber single spin flip dynamics [22]: at each update step, the flip is accepted if $\mathcal{H}$ decreases and rejected if $\mathcal{H}$ increases. The spins are updated until no spin flip can further decrease $\mathcal{H}$. At this point, the system has found a local minimum of $\mathcal{H}$, known as a metastable state. Note that this state is not necessarily the ground state, which is the global minimum of $\mathcal{H}$.

Metastable states are especially relevant to physical systems near phase transitions, including supercooled liquids [23] and atmospheric aerosol particles [24]. On a short time scale, the system appears to be at an equilibrium state, but on longer time scales, it undergoes transitions between different metastable states [25]. For disordered Ising models, metastable states have been realized experimentally in, for example, doped manganites [26] and colossal magnetoresistive manganites [27]. Despite their importance, there are many unresolved issues concerning metastable states [22], with analytical results largely restricted to one-dimension [28].

3. Random field Ising model

The key factor controlling melt pond configurations is the pre-melt sea ice topography, represented by random variables h_i. In the spirit of creating order from disorder, these variables are assumed to be independent Gaussian with zero mean and unit variance. The lattice constant $a = 1$ m is specified as the length scale above which important spatially correlated fluctuations occur in the power spectrum of sea ice topography (see supplementary materials available online at stacks.iop.org/NJP/21/063029/mmedia). We use the following update rule for Glauber dynamics, depending on whether there is a majority among the four nearest neighbors of a chosen site. If a majority exists, the site is updated to align with the majority due to heat diffusion between neighboring sites. Otherwise, we introduce a *tiebreaker* rule that describes the tendency for water to fill troughs: the chosen site is updated to ice if its pre-melt ice height is positive, and water otherwise; see figure 1(b). This update rule does not depend on any parameters other than h_i.

The above update rule can be restated as minimizing the classical RFIM free energy [29, 30]

$$\mathcal{H} = \sum_i (h_i - H) s_i - \sum_{\langle i,j\rangle} J s_i s_j, \tag{2}$$

with the uniformly applied field $H = 0$ and the coupling constant $J \to +\infty$; see supplementary materials for a brief discussion of the $H \neq 0$ case. To facilitate comparison with geophysical observations, the order parameter will be taken as the pond fraction F, which is defined as the fraction of up spins and therefore related to the magnetization M by $F = (M + 1)/2$. At $J = 0$, there is a unique metastable state, namely the ground state, given by $s_i = +1$ if $h_i < H$, and $s_i = -1$ if $h_i > H$. This process can only yield the correct melt pond geometry if the random variables h_i are highly correlated [16]. As J increases, metastable states appear [31] at a wider range of pond fractions, with the entire range $F \in [0,\ 1]$ covered for large enough J. As $J \to +\infty$, the two ground states are given by $s_i = +1$ or $s_i = -1$ for all i.

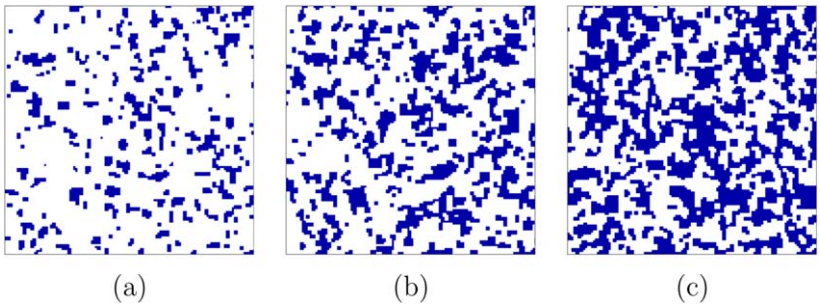

Figure 2. Melt ponds as metastable *islands* of like spins in our random field Ising model. Simulation results are shown for metastable states of the RFIM at $H = 0$ and $J = 5$. The output spin configurations are shown on a 128×128 portion of the 1024×1024 lattice with (a) $F_{\rm out} = 0.15$; (b) $F_{\rm out} = 0.30$; (c) $F_{\rm out} = 0.45$. Pixels are colored blue for water ($s_i = +1$) and white for ice ($s_i = -1$).

4. Geometry of metastable states

Below we present numerical results for the zero temperature Glauber dynamics of the RFIM, with the lattice size taken to be 1024×1024. The input spin configurations s_i are independent binary variables (Bernoulli trials) that equal $+1$ with probability $F_{\rm in}$ and -1 with probability $1 - F_{\rm in}$, where $F_{\rm in}$ denotes the input pond fraction. Note that these variables are uncorrelated with the h_i. Following a random update sequence, the Glauber dynamics eventually yield a metastable state with output pond fraction $F_{\rm out}$. Note that this metastable state is generically distinct from the two ground states unless $F_{\rm in} = 0$ or 1. Figure 2 shows the output configurations with $F_{\rm out} = 0.15, 0.30$, and 0.45, which respectively result from $F_{\rm in} = 0.34, 0.42$, and 0.48. This metastability is consistent with previous findings from a dynamical systems analysis [32].

The visual resemblance between the simulations in figures 2(a), (c) and the photos in figure 1(a) is now apparent, particularly in the well developed ponds where the minimum energy configurations of the model are quite evolved, coarse-grained and 'pond-like' in comparison to the purely random initial states. In the following we will analyze in detail the up spin clusters in figure 2(c) at $F_{\rm out} = 0.45$.

Figure 3(a) shows the log–log plot of the perimeter P versus the area A for these clusters (shown in physical units as Pa and Aa^2). Figure 3(b) shows the pond size distribution function prob(A). It exhibits power law scaling prob$(A) \sim A^{\zeta}$ with the exponent $\zeta = -1.58 \pm 0.03$ for pond areas in the range $10\ {\rm m}^2 < A < 1000\ {\rm m}^2$, in excellent agreement with the observed value [11] of about $-3/2$.

A key feature of multi-cluster systems is the tendency for smaller clusters to have simple shapes and larger clusters to have complex shapes. This onset of complexity can be quantified by an increase in the fractal dimension D, defined in terms of the perimeter P and the area A as $P \sim \sqrt{A}^{D}$. The input spin configuration corresponds to a site percolation process with occupation probability $F_{\rm in} < 0.5$, below the site percolation threshold of about 0.593 [33]. The Ising model takes these purely random states as input and produces the metastable states represented by the cloud of points in figure 3(a). The upper edge of this cloud has an almost constant fractal dimension close to the theoretical value of $91/48 \approx 1.896$ for site percolation clusters right below the percolation threshold [33]. Therefore, this upper edge represents the unphysical clusters reminiscent of the original input, which are least affected by the Glauber dynamics. To identify the physical clusters that resemble real melt ponds, we thus choose the lower edge, or equivalently the smallest possible P for each A, as highlighted in figure 3(a). Within this data set, we further exclude both the smaller ponds with $A < 15\ {\rm m}^2$ which are affected by the discreteness of the lattice, and the larger ponds with $A > 400\ {\rm m}^2$ which are subject to substantial sampling variability because of their rareness.

Figure 3(c) compares our Ising model $D(A)$ function (thin solid black curve) with the observed fractal dimension dependence on area for real melt ponds (thick gray data curve) [12]. The model thin black curve is a best fit to the data points in the (A, P)-plane for model ponds, as in [16]. From this best fit curve we find that the transition happens around the inflection point $A_c a^2 \approx 90\ {\rm m}^2$. This predicted value agrees well with the observed value [12] of about $100\ {\rm m}^2$, with the full observed $D(A)$ for real ponds reproduced in figure 3(d). The width of the transition regime in $\log(A)$ in figure 3(c) also agrees well with figure 3(d). Finally, supplementary figure 2 displays another quantifier of the onset of complexity that accounts for the entire collection of points in the (A, P)-plane. It yields the same critical transition area as before.

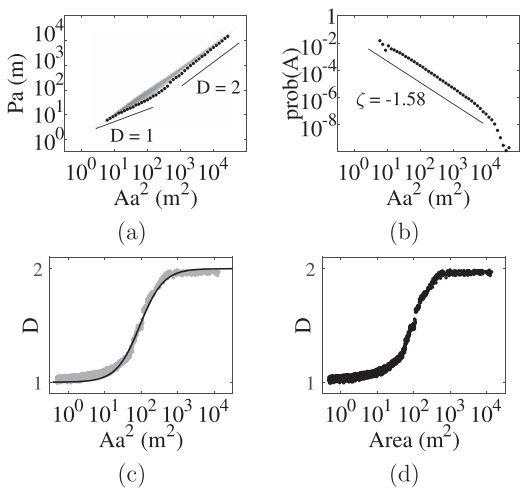

Figure 3. Geometrical characteristics of Ising model melt ponds. Simulation data in this figure are for the up-spin clusters in figure 2(c). (a) Log–log plot of the perimeter P versus the area A, rendered as a (rescaled) density plot. The lower edge of this cloud of points, highlighted by filled black circles, is determined by dividing $\log(A)$ into bins of size 0.2 and computing the minimum of $\log(P)$ for each bin. The reference lines have slopes 0.5 and 1, which correspond respectively to the fractal dimensions $D = 1$ and $D = 2$. (b) Log–log plot of the pond size distribution function $\mathrm{prob}(A)$, with bin size 0.2 and very small ponds with $A < 5$ m^2 excluded. The reference line has slope -1.58. (c) Plot of the fractal dimension D as a function of A (log scale) for our melt pond Ising model (thin solid curve) compared with the data curve (gray) for real melt ponds in (d) [12]. The solid curve is computed by fitting a suitable smooth function to the lower edge of the data points in panel (a) within the range 15 m^2 $< A <$ 400 m^2. (d) (Reproduced [12] with permission.) Fractal dimension as a function of area (log scale) based on image analysis of real melt ponds [12]. In panels (a)–(c), A and P are shown in physical units with the lattice constant $a = 1$ m, and the number of sites is increased to 8192 $\times$ 8192 to improve the statistics.

5. A scheme for more realistic pond boundaries

One discrepancy with observations is that our smaller model ponds are non-Euclidean on average, namely that they have an average fractal dimension greater than 1 (see figure 2(c)). To address this issue and better describe the physical process of melt pond formation, we can allow the ice topography h_i to co-evolve with the spin configuration s_i. A possible evolution scheme is outlined next.

Let us introduce a discrete time index n, and denote the ice topography and the spin configuration at time n respectively by h_i^n and s_i^n. The evolution from time n to time $n + 1$ proceeds as follows. First, s_i^{n+1} is determined as before by minimizing the RFIM free energy $\mathcal{H}$, with h_i^n being the pre-melt ice topography and s_i^n being the input spin configuration. Second, h_i^{n+1} is determined by the following formula

$$h_i^{n+1} = f(n, h_i^n, s_i^n, s_i^{n+1}) + g_i^{n+1}, \tag{3}$$

where the function f and the random field g_i^{n+1} represent the deterministic and stochastic mechanisms of the topography evolution, encompassing internal processes of melting and freezing, as well as external influences such as environmental forcing, drainage processes, seasonal patterns, etc. In this evolution scheme, the system transitions between metastable states of an evolving free energy landscape, with the equilibration time estimated to be 4–5 d (see supplementary materials).

Here, instead of proposing a realistic expression for the function f, we simply consider $f = 0$ for illustration purposes. In this case, the h_i^n at successive time steps $n = 0, 1, 2, \cdots$ are independent (in both space and time) Gaussian variables with zero mean and unit variance. As shown in figure 4, the boundaries become smoother as n increases. As a result, the fractal dimensions of the smaller ponds become closer to 1, while for the larger ponds it remains close to 2, as is evident from comparing figures 3(a) and 4(e). The shapes of the simulated ponds in figure 4(b) closely resemble those of the observed melt ponds in figure 4(d). The power law scaling exponent of the pond size distribution function is found to be $\zeta = -1.71 \pm 0.02$, as shown in figure 4(f).

6. Discussion

Our melt pond Ising model—with only one measured input parameter—produces ponds that are not only quite realistic in appearance, but with geometrical characteristics that quantitatively match very closely the observations on pond sizes and fractal dimension. This one parameter sets the length of a side of a square pixel in the lattice, and represents the scale above which the variations in snow topography are significant. Moreover, as

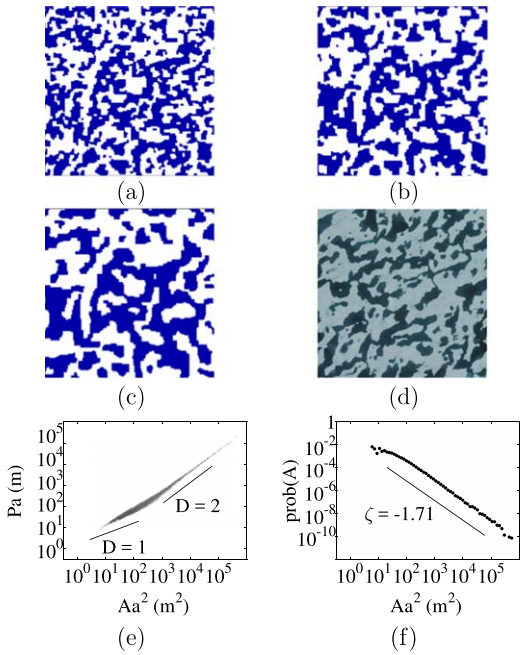

Figure 4. Time evolution of metastable states with an evolving ice topography. Simulation results are shown for metastable states of the RFIM at $H = 0$ and $J = 10$. The h_i^n at $n = 0, 1, 2, \cdots$ are assumed to be independent Gaussian variables with zero mean and unit variance. The input configuration s_i^0 has pond fraction $F_{\text{in}} = 0.495$. The output configurations s_i^n are shown on a 165×165 lattice at (a) $n = 2$; (b) $n = 4$; (c) $n = 8$. Pixels are colored blue for water ($s_i = +1$) and white for ice ($s_i = -1$). (d) Aerial image of Arctic melt ponds. Each side of this photo is 165 m. Panels (e), (f) show the geometric characteristics of the up-spin clusters in panel (b). (e) Log–log plot of the perimeter P versus the area A, rendered as a (rescaled) density plot. The reference lines are at the same location as those in figure 3(a) to facilitate comparison. (f) Log–log plot of the pond size distribution function prob(A), with bin size 0.2 and very small ponds with $A < 5$ m^2 excluded. The reference line has slope -1.71.

energy is minimized via Glauber dynamics the model creates *order from disorder*, flowing from a random initial state to a configuration with long range order.

The description of complex melt ponds in terms of a simple disordered system may well advance our ability to model the future trajectory of the Arctic sea ice pack, e.g. through parameterizations in climate models. Our approach based on energy minimization in statistical mechanics potentially opens new avenues for incorporating ponds, particularly in higher resolution, micro- and meso-scale models for regions up to hundreds of kilometers across. Efficient numerical algorithms which yield not only melt water volume but fast, accurate information about how it is distributed—based on the ambient conditions, would be broadly useful in sea ice dynamics, thermodynamics, and ecology. Assumptions about melt pond spatial structure influence the sub-grid scale spatial pattern of melt pond depths, meaning how water is distributed over the sea ice thickness distribution. These variations in water depth in turn markedly impact grid scale albedo.

The basic model presented here can be augmented to incorporate more detailed processes, such as the effect of changes in snow topography—potentially relevant in a changing climate. For example, effects of anisotropy in the topography can be included, as was studied in detail in [16]. The melt pond Ising model also offers the potential for efficient yet geometrically sophisticated parameterizations of melt ponds and their impact in climate models, as well as more refined models of sea ice physics and biology. In addition, the statistical physics approach developed here may be generalizable to other systems near the transition point between ice and water, such as tundra permafrost lakes, where the melting front has been described using a curve-shortening flow [34].

Minimal models such as the RFIM necessarily have limitations. Mathematically, the geometry of a fractal cannot be fully captured by its interpolation on a lattice. Physically, the RFIM is inherently unable to resolve processes at length scales smaller than the lattice constant. There, one may expect narrow water channels responsible for connecting smaller ponds into larger ponds. The inability to resolve such features likely causes the percolation threshold of the RFIM to differ from observations. For the metastable states obtained from random inputs, the percolation threshold is very close to 0.5 at $H = 0$ (see supplementary materials). This threshold decreases as H decreases, but likely always exceeds the value for real melt ponds.

Acknowledgments

We gratefully acknowledge support from the Division of Mathematical Sciences and the Division of Polar Programs at the US National Science Foundation (NSF) through Grants DMS-1009704, ARC-0934721, DMS-0940249, DMS-1413454, and DMS-0940262. We are also grateful for support from the Arctic and Global Prediction Program and the Applied and Computational Analysis Program at the US Office of Naval Research through grants N00014-13-10291, N00014-15-1-2455, N00014-18-1-2041, and N00014-18-1-2552. YM acknowledges support from a Vice Chancellor's Research Fellowship at Northumbria University. IS acknowledges support from the RFBR under the Grant #16-31-60070 mol_a_dk. Finally, we would like to thank the NSF Math Climate Research Network (MCRN) for their support of this work.

ORCID iDs

Yi-Ping Ma https://orcid.org/0000-0002-7584-2734
Ivan Sudakov https://orcid.org/0000-0003-2614-8794
Courtenay Strong https://orcid.org/0000-0001-5866-4377

References

[1] Flocco D, Feltham D L and Turner A K 2010 Incorporation of a physically based melt pond scheme into the sea ice component of a climate model *J. Geophys. Res.* **115** C08012
[2] Perovich D K and Polashenski C 2012 Albedo evolution of seasonal Arctic sea ice *Geophys. Res. Lett.* **39** L08501
[3] Polashenski C, Perovich D and Courville Z 2012 The mechanisms of sea ice melt pond formation and evolution *J. Geophys. Res.* **117** C01001
[4] Schröder D, Feltham D L, Flocco D and Tsamados M 2014 September Arctic sea-ice minimum predicted by spring melt-pond fraction *Nat. Clim. Change* **4** 353–7
[5] Scott F and Feltham D L 2010 A model of the three-dimensional evolution of Arctic melt ponds on first-year and multiyear sea ice *J. Geophys. Res.* **115** C12064
[6] Perovich D K, Richter-Menge J A, Jones K F and Light B 2008 Sunlight, water, and ice: extreme Arctic sea ice melt during the summer of 2007 *Geophys. Res. Lett.* **35** L11501
[7] Flocco D, Schroeder D, Feltham D L and Hunke E C 2012 Impact of melt ponds on Arctic sea ice simulations from 1990 to 2007 *J. Geophys. Res.* **117** C09032
[8] Arrigo K R *et al* 2012 Massive phytoplankton blooms under Arctic sea ice *Science* **336** 1408
[9] Horvat C, Jones D R, Iams S, Schroeder D, Flocco D and Feltham D 2017 The frequency and extent of sub-ice phytoplankton blooms in the Arctic Ocean *Sci. Adv.* **3** e1601191
[10] Nicolaus M, Katlein C, Maslanik J and Hendricks S 2012 Changes in Arctic sea ice result in increasing light transmittance and absorption *Geophys. Res. Lett.* **39** L24501
[11] Perovich D K, Tucker W B and Ligett K 2002 Aerial observations of the evolution of ice surface conditions during summer *J. Geophys. Res.* **107** C000449
[12] Hohenegger C, Alali B, Steffen K R, Perovich D K and Golden K M 2012 Transition in the fractal geometry of Arctic melt ponds *Cryosphere* **6** 1157–62
[13] Christensen K and Moloney N R 2005 *Complexity and Criticality* (London: Imperial College Press)
[14] Isichenko M B 1992 Percolation, statistical topography, and transport in random media *Rev. Mod. Phys.* **64** 961–1043
[15] Torquato S 2002 *Random Heterogeneous Materials: Microstructure and Macroscopic Properties* (Berlin: Springer)
[16] Bowen B, Strong C and Golden K M 2018 Modeling the fractal geometry of Arctic melt ponds using the level sets of random surfaces *J. Fract. Geom.* **5** 121–42
[17] Popović P, Cael B B, Silber M and Abbot D S 2018 Simple rules govern the patterns of Arctic sea ice melt ponds *Phys. Rev. Lett.* **120** 148701
[18] Yeomans J M 1992 *Statistical Mechanics of Phase Transitions* (Oxford: Clarendon)
[19] Milton G W 2002 *The Theory of Composites, Cambridge Monographs on Applied and Computational Mathematics* vol 6 (Cambridge: Cambridge University Press)
[20] Khouider B, Majda A J and Katsoulakis M A 2003 Coarse-grained stochastic models for tropical convection and climate *Proc. Natl Acad. Sci. USA* **100** 11941–6
[21] Young A P 1998 *Spin Glasses and Random Fields* (Singapore: World Scientific)
[22] Krapivsky P L, Redner S and Ben-Naim E 2010 *A Kinetic View of Statistical Physics* (Cambridge: Cambridge University Press)
[23] Büchner S and Heuer A 2000 Metastable states as a key to the dynamics of supercooled liquids *Phys. Rev. Lett.* **84** 2168–71
[24] Rood M, Shaw M, Larson T and Covert D 1989 Ubiquitous nature of ambient metastable aerosol *Nature* **337** 537–9
[25] Langer J S 1969 Statistical theory of the decay of metastable states *Ann. Phys.* **54** 258–75
[26] Moreo A, Mayr M, Feiguin A, Yunoki S and Dagotto E 2000 Giant cluster coexistence in doped manganites and other compounds *Phys. Rev. Lett.* **84** 5568–71
[27] Wu W, Israel C, Hur N, Park S, Cheong S-W and De Lozanne A 2006 Magnetic imaging of a supercooling glass transition in a weakly disordered ferromagnet *Nat. Mater.* **5** 881–6
[28] Derrida B and Gardner E 1986 Metastable states of a spin glass chain at 0 temperature *J. Phys.* **47** 959–65
[29] Andelman D and Joanny J-F 1985 Metastability in the random-field Ising model *Phys. Rev.* B **32** 4818–21
[30] Perez-Reche F J, Rosinberg M L and Tarjus G 2008 Numerical approach to metastable states in the zero-temperature random-field Ising model *Phys. Rev.* B **77** 064422
[31] Wu Y and Machta J 2005 Ground states and thermal states of the random field Ising model *Phys. Rev. Lett.* **95** 137208

[32] Sudakov I, Vakulenko S A and Golden K M 2015 Arctic melt ponds and bifurcations in the climate system *Commun. Nonlinear Sci. Numer. Simul.* **22** 81
[33] Stauffer D and Aharony A 2014 *Introduction to Percolation Theory: Revised* 2nd edn (Boca Raton, FL: CRC Press)
[34] Sudakov I and Vakulenko S A 2015 A mathematical model for a positive permafrost carbon-climate feedback *IMA J. Appl. Math.* **80** 811–24

Supplementary Materials for "Ising model for melt ponds on Arctic sea ice"

Spatial scale from snow topography data. — The lattice constant a must be small relative to the 10-20 m length scales prominent in sea ice and snow topography [35]. We set $a = 1$ m as the length above which the power spectral density (psd) of observed snow topography exceeds a null red noise spectrum (Supplementary Fig. 1). For this calculation, we used 13 radar transects collected during the Surface Heat Budget of the Arctic Ocean (SHEBA) project [36]. To estimate the psd via the Welch modified periodogram, we calculated the power spectrum for each transect with a Hanning window and 50% segment overlap, and then averaged the results across the transects. We calculated the corresponding null red noise spectrum based on lag-one spatial autocorrelation [37] averaged across the transects.

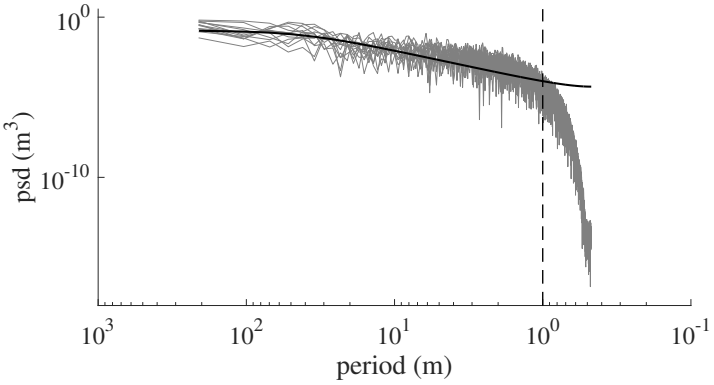

Supplementary Figure 1. Snow depth power spectral density (gray curve) with corresponding null red noise spectrum (black curve). The lattice constant $a = 1$ m is indicated by a vertical dashed line.

Temporal scale from vertical energy balance. — The melt pond system can be modeled as a thin active layer on top of the bulk sea ice floe, subject to incoming and outgoing radiation and heat exchange with the bulk. Let R_+ be the net radiation received by water, and R_- be the net radiation received by ice:

$$R_+ = \mathrm{ISR}_+ - \mathrm{OLR}, \quad R_- = \mathrm{ISR}_- - \mathrm{OLR}, \tag{S1}$$

where ISR and OLR respectively represent the incoming shortwave radiation and the outgoing longwave radiation. The former is $\mathrm{ISR}_+ = Q(1-\alpha_+)$ and $\mathrm{ISR}_- = Q(1-\alpha_-)$, where $Q = 460\ \mathrm{W \cdot m^{-2}}$ is the mean solar insolation during polar summer, and α is the surface albedo with $\alpha_+ = 0.1$ for water and $\alpha_- = 0.5$ for ice. The latter is $\mathrm{OLR} = \sigma(T + 273)^4$, where $\sigma = 5.67 \times 10^{-8}\ \mathrm{W \cdot m^{-2} K^{-4}}$ is the Stefan-Boltzmann constant, and the temperature $T \approx 0$ Celsius for both water and ice. Therefore we obtain $R_+ = 99\ \mathrm{W \cdot m^{-2}}$ and $R_- = -85\ \mathrm{W \cdot m^{-2}}$.

Bulk sea ice as a porous composite of brine and ice on the microscopic scale often has a temperature just below zero Celsius during the melt season. Meanwhile, the heat transfer between the bulk sea ice and the active layer of melt ponds is known to be very efficient. As a result, a patch of water in the active layer always has a temperature

slightly above zero Celsius due to the positivity of R_+, and a patch of ice in the active layer always has a temperature slightly below zero Celsius due to the negativity of R_-.

If external influences such as surface topography and interactions with the surroundings are present, a patch of water in the active layer can transition into ice, and vice versa. We assume that the transition of a patch of water to ice is facilitated by changing the net radiation from R_+ to R_-, and that the transition of a patch of ice to water is facilitated by changing the net radiation from R_- to R_+. The required energies per unit area to freeze water and to melt ice are respectively $E_+ = -L\rho_+ h$ and $E_- = L\rho_- h$, where $L = 3.34 \times 10^5\ \mathrm{J \cdot kg^{-1}}$ is the latent heat of fusion, $\rho_+ = 1 \times 10^3\ \mathrm{kg \cdot m^{-3}}$ is the density of water, $\rho_- = 9.2 \times 10^2\ \mathrm{kg \cdot m^{-3}}$ is the density of ice, and $h = 0.1$ m is a realistic value for the height of the active layer. Therefore, the time scales required to freeze water and to melt ice under these assumptions are respectively $\tau_{w\to i} = E_+/R_- = 5$ days and $\tau_{i\to w} = E_-/R_+ = 4$ days. For example, this rough estimate gives a time scale of about 20 days, or 4 steps of spin flipping, for a well-developed network of ponds like those in Fig. 4(b) to evolve, which is reasonable.

Alternative quantifier of the onset of complexity. — To account for the entire cluster of points in the (A, P)-plane in Fig. 3(a), we define a new quantifier of the onset of complexity as the variance σ of $\log(P)$, hereafter referred to as the *elasticity*. As shown in Supplementary Fig. 2, there exists a critical area A_c such that $\sigma(\log(P))$ increases with $\log(A)$ for simple ponds with $A < A_c$, and decreases with $\log(A)$ for complex ponds with $A > A_c$. The onset of complexity may then be identified with maximum elasticity, which occurs at $A_c a^2 \approx 90\ \mathrm{m}^2$. This coincides with the critical area determined from Fig. 3(c) by the inflection point in the best fit.

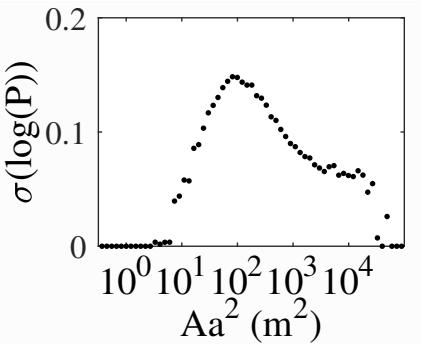

Supplementary Figure 2. Plot of the variance $\sigma(\log(P))$ as a function of A (log scale), with bin size 0.2. The maximum occurs at $A_c a^2 \approx 90\ \mathrm{m}^2$.

Percolation threshold and correlation length exponent. — For a two dimensional square lattice with occupation probability p, the site-site correlation function $g(r_i, r_j)$ gives the probability that a site at r_j is a member of the same cluster as a site at r_i. The function g is assumed to decay with large distance $d = |r_i - r_j|$ according to

$$g(d) \sim \exp\left(-\frac{d}{\xi(p)}\right), \tag{S2}$$

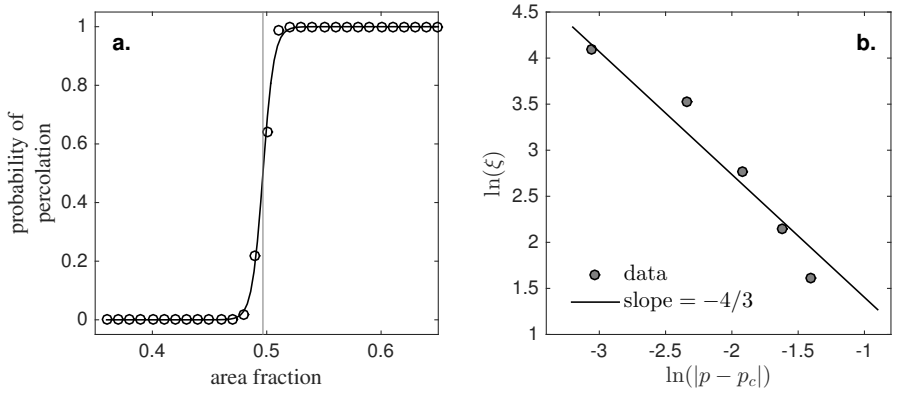

Supplementary Figure 3. (a) Probability of percolation as a function of area fraction. The curve is a hyperbolic tangent fit with inflection point close to 0.5 indicating the percolation threshold p_c. (b) Comparison of output from the Ising model (filled circles) to the line with slope $-\nu = -4/3$ given by the universal correlation length exponent ν.

where $\xi(p)$ is referred to as the correlation length. Theory indicates that $\xi(p)$ should obey

$$\ln \xi(p) \sim -\nu \ln(|p - p_c|), \quad p \longrightarrow p_c^-, \tag{S3}$$

where $\nu = 4/3$ is the universal critical exponent in two dimensions and p_c is the percolation threshold. For the two-dimensional square site lattice, $p_c \approx 0.59274621$ [38]. For the RFIM, analysis of 5,000 model realizations on 1024×1024 lattices yields a value close to $p_c = 0.5$ (Fig. 3a), with correlation lengths aligning reasonably with the universal exponent $\nu = 4/3$ (Fig. 3b). This result indicates that the spatial correlation structure of melt ponds in this model is sufficiently short-ranged so that the system falls within a standard universality class [15].

Nonzero uniformly applied field. — Let us choose $H \neq 0$ and keep $J \to +\infty$ in the RFIM given by Eq. (2). Then the tiebreaker rule for a chosen site i changes to $s_i = +1$ if $h_i < H$, and $s_i = -1$ if $h_i > H$, which favors ice for $H < 0$ and water for $H > 0$. Here we only consider two limiting cases when the tiebreaker rule completely favors ice or water: (I) $0 \ll -H \ll J$; (II) $0 \ll H \ll J$. In these cases, the random field h_i does not affect the kinetics, so the RFIM reduces to the classical Ising model without disorder,

$$\mathcal{H} = -H \sum_i s_i - J \sum_{\langle i,j \rangle} s_i s_j. \tag{S4}$$

The corresponding metastable states are known as Wulff droplets [39]. In case (I) the up-spin clusters are more elongated, and the percolation threshold is below 0.5. In case (II) the up-spin clusters are more circular, and the percolation threshold is above 0.5. These geometrical features afforded by varying H (and possibly also J) provide additional prospects to describe detailed shapes of real melt pond patterns.

Alternative update rule and free energy. — Let us retain the RFIM update rule when a majority exists among the neighboring sites, but adopt the following tiebreaker

rule: the chosen site is updated to ice if its pre-melt ice height is larger than the average between the two neighboring ice sites, and water otherwise. For example, in Fig. 1(b) we require that $s_P = +1$ if $h_P < (h_B + h_C)/2$, and -1 otherwise. This new update rule can be restated as minimizing an interfacial energy between water and ice: if a water site i neighbors an ice site j, then a penalty $W - h_j$ is imposed, where $W \gg 0$ is a constant. The total free energy $\mathcal{H}$ can then be written in two equivalent forms,

$$\mathcal{H} = \sum_{\langle i,j\rangle : s_i>0,\, s_j<0} (W - h_j) \equiv \sum_i s_i \Delta_i h - \sum_{\langle i,j\rangle} \frac{1}{2} s_i s_j (W - \Omega_{ij} h), \tag{S5}$$

where Δ_i and Ω_{ij} represent, respectively, the discrete Laplacian at site i and the average between sites i, j,

$$\Delta_i h \equiv h_i - \frac{1}{4} \sum_{j:\langle i,j\rangle} h_j, \quad \Omega_{ij} h \equiv \frac{1}{2}(h_i + h_j). \tag{S6}$$

The new "effective" random fields $\Delta_i h$, being the curvature of h_i, are more correlated than the h_i by themselves. As a result, at output pond fraction $F_{out} = 0.45$, the critical area for the transition in fractal dimension and the critical area for maximum elasticity are both $A_c a^2 \approx 120$ m^2. The corresponding power law scaling exponent for the pond size distribution is $\zeta = -1.57 \pm 0.03$.

References

[35] C. Petrich, H. Eicken, C. M. Polashenski, M. Sturm, J. P. Harbeck, D. K. Perovich, and D. C. Finnegan. Snow dunes: A controlling factor of melt pond distribution on Arctic sea ice. *J. Geophys. Res.*, 117:C09029, 2012.

[36] M. Sturm, J. Holmgren, and D. K. Perovich. Winter snow cover on the sea ice of the Arctic Ocean at the Surface Heat Budget of the Arctic Ocean (SHEBA): Temporal evolution and spatial variability. *J. Geophys. Res.*, 107(C10):C000400, 2002.

[37] D. L. Gilman, F. J. Fuglister, and J. M. Mitchell. On the power spectrum of red noise. *J. Atmos. Sci.*, 20(2):182–184, 1963.

[38] M. E. J. Newman and R. M. Ziff. Efficient Monte Carlo algorithm and high-precision results for percolation. *Phys. Rev. Lett.*, 85:4104–4107, 2000.

[39] R. H. Schonmann and S. B. Shlosman. Wulff droplets and the metastable relaxation of kinetic Ising models. *Commun. Math. Phys.*, 194(2):389–462, 1998.